Pre- and Post-Sea-Breeze Frontal Lines—A Meso-γ-Scale Analysis over South Israel

P. ALPERT AND M. RABINOVICH-HADAR

Department of Geophysics and Planetary Sciences, Raymond and Beverly Sackler Faculty of Exact Sciences, Tel Aviv University, Tel Aviv, Israel

(Manuscript received 26 April 2002, in final form 22 May 2003)

ABSTRACT

A meso-γ-scale observational analysis of the fine surface structure of the sea-breeze fronts (SBF) over the coast of southern Israel is presented. Objective criteria for the SBF passage are derived based on wind speed and direction, temperature, and humidity. A realization of an automized detection system for SBF is described.

Preliminary results indicate that, in addition to the primary SBF, there are significant and consistent pre- and post-SBF lines. The surface structures of these lines are shown, and related to earlier theoretical studies of the SBF forerunners and Kelvin–Helmholz waves.

Although the pre- and post-SBF lines seem to be important for pollutant transport, human comfort, and better theoretical understanding of the SBF, they have previously attracted little attention in the SBF literature.

1. Introduction

A vast literature exists on the characteristics of the sea-breeze front (SBF) based on observations, for example, Atkinson (1981) and Simpson (1994). Until the 1940s, the focus was on surface or near-surface measurements, and since then, the upper-level circulation of the SBF has also been explored with the aid of balloons, airplanes, radar, satellite, Doppler-radar, and more recently, theoretical and/or numerical models, for example, Kimble (1946), Haurwitz (1947), Pearce (1955), Estoque (1962), Neumann and Mahrer (1971, 1974), Simpson et al. (1977), Alpert et al. (1982), and Wakimoto and Atkins (1994). A more recent summary of the sea-breeze and local winds is given by Simpson (1994).

The SBF has been identified from a change in wind direction, an increase of wind speed, a drop in temperature and an increase of humidity, associated with the arrival of the relatively cool and humid sea air mass, for example, Atkinson (1981, Fig. 59). Other possible identifiers are a drop of virtual temperature or an increase of the dew point or the equivalent potential temperature (Wakimoto and Atkins 1993). The intensity of these changes varies with place, season, and latitude. In India and Israel, for instance, the average SBF wind speed increase is 4–5 m s^{-1} and temperature drop is 1°–5°C. Normally, the Northern Hemispheric rotation of the wind direction is clockwise due to the Coriolis force as shown by Neumann (1977). In some locations, however, rotation could be in the anticlockwise sense (Staley 1957; Alpert et al. 1984). Kusuda and Alpert (1983) have attributed this to an additional pressure-gradient forcing out of phase with that of the SBF sometimes acting even parallel to the seashore line. Such a force may be due to topography.

Several studies have focused on the horizontal and vertical propagation of the SBF, for cases in Australia (Clarke 1955), in California (Schroeder et al. 1967), or in England (Simpson et al. 1977). Others have investigated the effects of a synoptic flow, for example, Estoque (1962), Helmis et al. (1987), Arritt (1993), and Wakimoto and Atkins (1993).

In Israel, a number of pioneering theoretical studies on the SBF were performed by Neumann and Mahrer (1971, 1974), Neumann (1977), Alpert et al. (1982), and Segal et al. (1985). A few studies, however, were oriented to observational analyses. Skibin and Hod (1979) performed subjective analyses of mesoscale flow patterns over north Israel. Alpert and Getenio (1988) and Alpert (1988) have combined surface wind observations with 3D and 2D model predictions in order to obtain the best description of the mesoscale summer flow characteristics in Israel. These observational studies, however, have not typically had time resolution of less than 3-h intervals of the observed synoptic data.

The purpose of the present study is first, to attempt to develop surface-based objective criteria for the detection of SBF with high temporal resolution data. Second, we explore the meso-γ-scale characteristics of the summer SBF in Israel, employing both a high temporal resolution (5 min) and a unique spatial (12 stations over 400 km^2) automatic net of environmental stations. In particular, attention is given to the evidence presented

Corresponding author address: Dr. Pinhas Alpert, Dept. of Geophysics and Planetary Sciences, Raymond and Beverly Sackler Faculty of Exact Sciences, Tel Aviv University, Ramat Aviv, Tel Aviv 69978, Israel.
E-mail: pinhas@cyclone.tau.ac.il

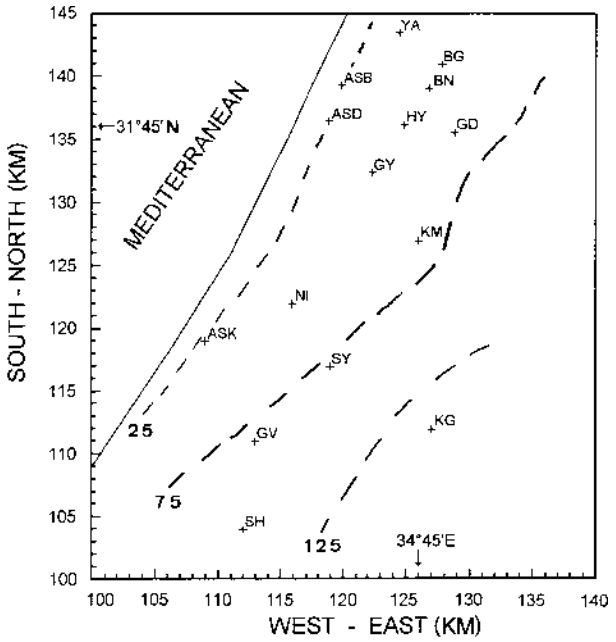

FIG. 1. Map of area with surface stations. Distances are in kilometers and local coordinates are indicated. Topographic contours (dashed) are for 25, 75, and 125 m. Stations are drawn from north to south: Yavne (YA), Bet Gamliel (BG), Ashdod Bazan (ASB), Benaya (BN), Ashdod (ASD), Hevel-Yavne (HY), Gedera (GD), Gan Yavne (GY), Kiryat Malachi (KM), Nir Israel (NI), Ashkelon (ASK), Sde-Yoav (SY), Kiryat Gat (KG), Gvaraam (GV), and Shderot (SH).

here for the existence of pre- and post-SBF lines over the south coast of Israel and their possible relationship with earlier theoretical predictions of SBF forerunners by Geisler and Bretherton (1969), and with the Kelvin–Helmholz (KH) waves following the SBF.

2. Methodology of observational analysis

a. Description of stations and data

Figure 1 shows a map of the study area over the southeast Mediterranean coast, Israel, and the 15 meteorological stations. This makes a dense net over an area 40 km long and 20 km wide. For 12 of the stations (excluding the most southern 3 stations), the average area per station is only about 33 km^2. Except for two stations in the north, [i.e., Ashdod Bazan (ASB) and Bet Gamliel (BG)], the stations are for environmental monitoring of the air downstream of the towns of Ashdod (ASD) and Ashkelon (ASK) where coal-based electric power plants are operating. Several years ago the air-quality was exceptionally low particularly downstream of Ashdod and the recent use of low-sulphur gasoline in certain synoptic situations based on advanced warnings has much improved the air-quality over this area. The stations automatically record wind speed and intensity, as well as temperature continuously, and 5-min averages are carried out. In the stations ASD, ASK, and Kiryat Gat (KG) additional parameters like humidity, pressure, global radiation, and rainfall are also measured. Pollutant concentrations of SO_2, NO_x, NO, and O_3 are also being measured at all the environmental stations. Basic quality control (QC) of the data was performed by the corresponding environment networks of Ashdod and Ashkelon. The QC is performed manually, and suspicious data were flagged as ''invalid'' (D. Lahav 2002, personal communication).

The two northern stations ASB and BG do not measure pollutants, but meteorological fields at a few levels. At the ASB tower, wind, temperature, and humidity measurements are taken at 2, 10, and 60 m, while at the BG tower (P. Alport's house), the temperature measurements at 0.5, 2, and 10 m are taken every 10 min.

Meteorological parameters that were found to be consistently anomalous or suspicious with erroneous reports (in spite of the environment QC system) are not employed in this study, even though some can still be used to detect SBFs. For instance, the humidity at ASD was consistently too low. Reasons for that may be improper positioning or nonstandard location or inaccurate calibration of the instrument. But, they may still be used sometimes, to identify the SBF arrival by the method described next.

b. Data analysis methodology

The summer day of the 20 July 1993 was chosen for preliminary analysis since most of the data was available. It was later found to present a well-developed SBF with weak synoptic forcing. The dominant synoptic summer pattern is a subtropical high over Israel along with a Persian trough to the north with typical west-northwest winds of about 2–5 m s^{-1} (Alpert et al. 1992). Early-morning low-level stratocumulus clouds frequently form, but quickly dissipate because of the strong subsidence.

The original 5-min average data were found to contain large fluctuations, reflecting the turbulence in vigorous large eddies that are typical for clear days with strong solar irradiation. Hence, five- and seven-point running averages (20 and 30 min, respectively) were found to be useful for the detection of the SBF by partly smoothing the turbulence. Figures 2–4 show the original 5-min data and the 20-min-averaged time series for wind direction (WD) (Fig. 2), wind speed (WS) (Fig. 3), and temperature (T) (Fig. 4) for the station Nir Israel (NI; Fig. 1). The original wind direction in Fig. 2a possesses high variability while the five-point smoothing in Fig. 2b clearly shows a steady and sharp clockwise wind turning between 1025 to 1045 local standard time (LST) from southerly 190° to westerly 260°. Similarly, the smoothed wind speed in Fig. 3b indicates a sharp increasing trend from 1.5 to 3.5 m s^{-1} during 1045 to 1115 LST. The original temperature time series, Fig. 4a, shows several times where the temperature stabilizes or even drops, namely, at 0850, 0950, 1035, and 1055 LST, but the smoothed plot, Fig. 4b, emphasizes the 1105 LST change in the temperature trend. From this time

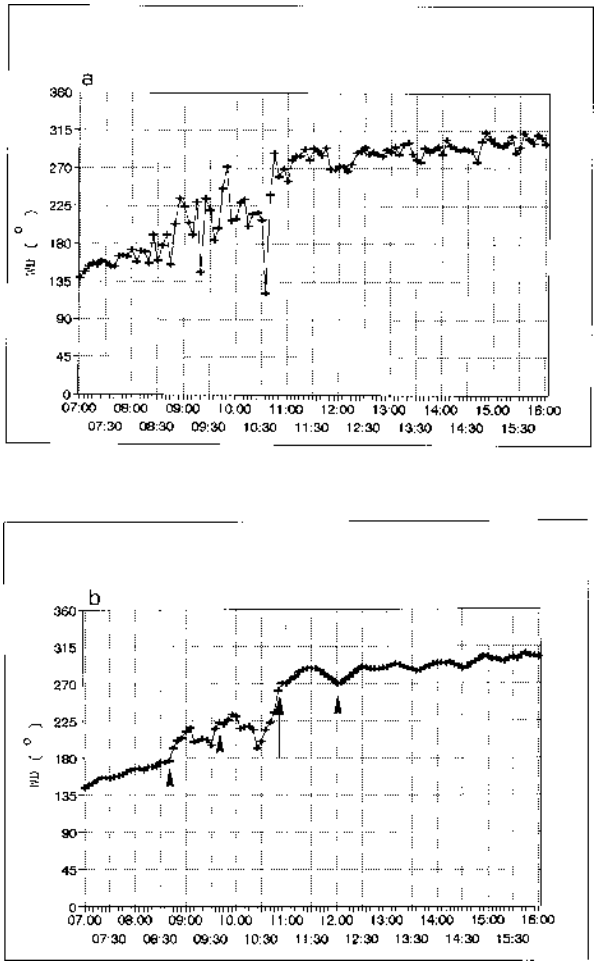

FIG. 2. Time series of WD (degrees) at NI on 20 Jul 1993. (a) Basic data at 5-min intervals, and (b) five-point running average. Arrow indicates SBF passage (see text). Abscissa indicates local time (LST), which is 3 h ahead of UTC time (summertime). Pre- and post-SBF lines (see section 4a) are indicated by arrowheads.

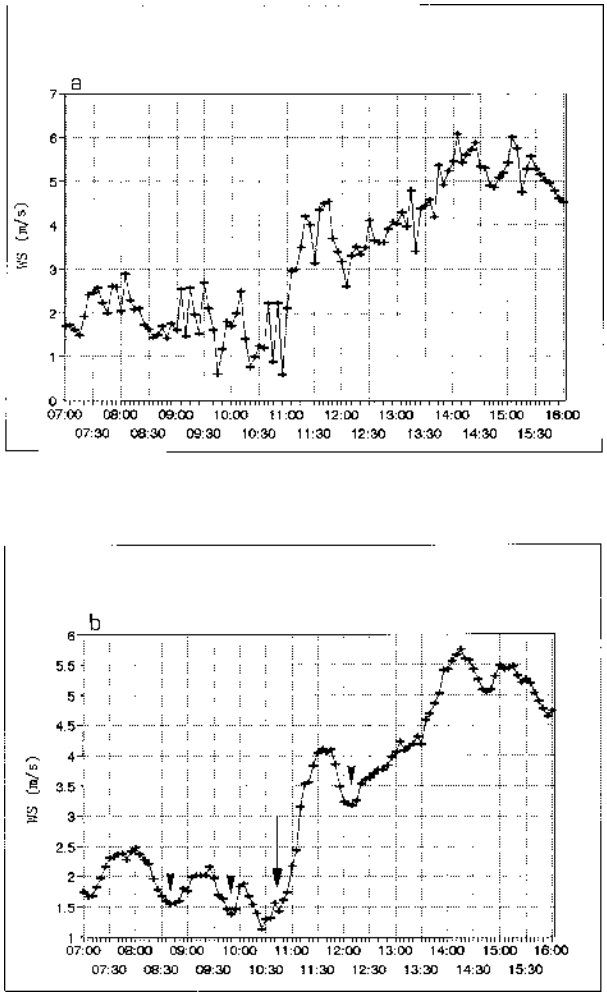

FIG. 3. As in Fig. 2, but for WS (m s^{-1}).

onward for about 50 min, the average temperature drops in spite of the continuing increase of the solar heating, clearly indicating the SBF arrival. The seven-point smoothing was also analyzed (Rabinovich-Hadar 1995) but not found necessary for the further analysis. The humidity variations were available only in four stations and will be discussed in section 3c.

3. Criteria for the SBF

a. Formulation of objective criteria for SBF arrival

A computer program was written in order to objectively calculate the SBF arrival points. This was based on a subjective inspection of the results for a period of 10 days during the summer for all the stations. The SBF arrival is accompanied by clockwise wind rotation, wind speed increase, temperature drop, and humidity increase. However, not all these signals appear in unison, since they depend on the SBF intensity and its stage of evolution. The decision to take either the beginning or end of the variation for a specific field was based on an attempt to fit the different SBF arrival times based on the various parameters into the shortest time span. A similar choice was made by Chiba (1993). Consequently, for all parameters other than the wind direction, the SBF time was chosen to be at the beginning of the change. This suggests (as discussed in section 3d) that the wind direction is a particularly sensitive parameter.

At the end of the inspection process the following criteria for SBF arrival were chosen based on the 20-min average data.

1) Wind direction. End of clockwise rotation (CWR) of at least 45° within 15 min. If such a wind turning was not found, then the largest CWR that extended for at least 15 min was used.
2) Wind speed. Beginning of a continuous wind increase of at least 1.5 m s^{-1} within 35 min. If such a temporal gradient was not found, then the largest increase that extended for at least 25 min was used.

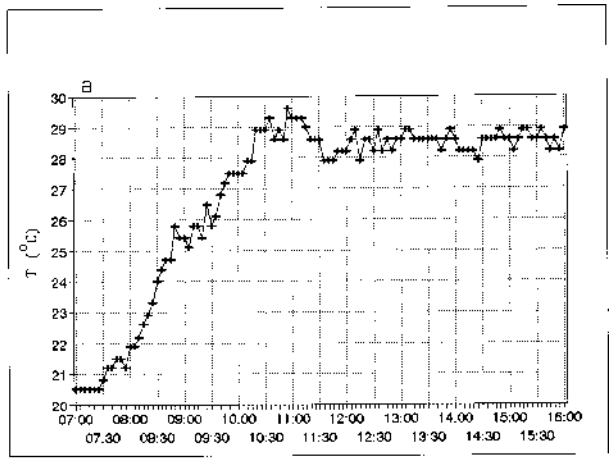

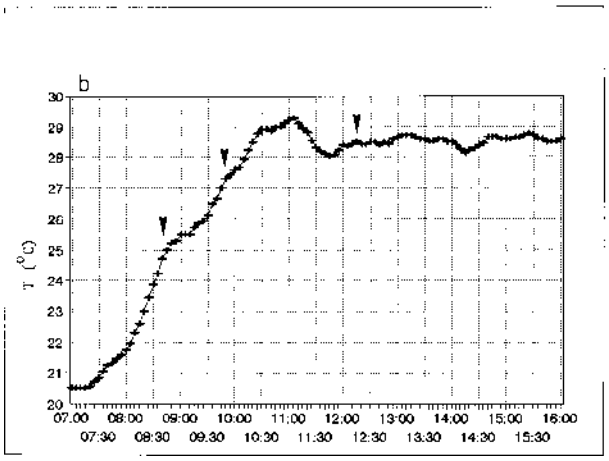

FIG. 4. As in Fig. 2, but for T (°C).

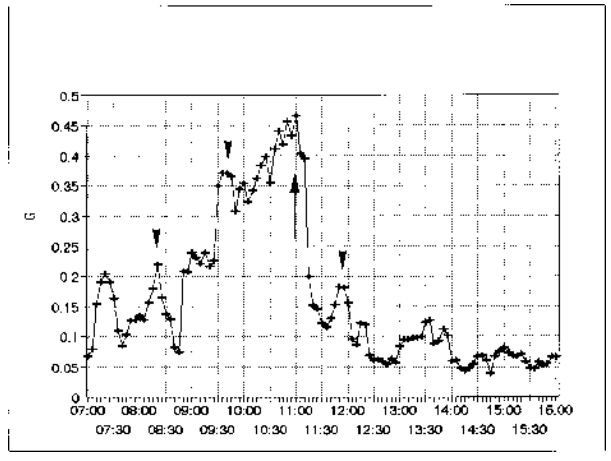

FIG. 5. Time series for gustiness G at station NI on 20 Jul 1993. Arrow and arrowheads indicate SBF and pre- or post-SBF lines as in Figs. 2–4.

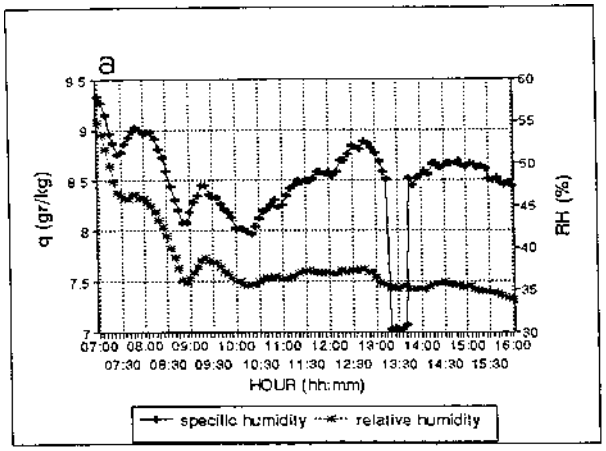

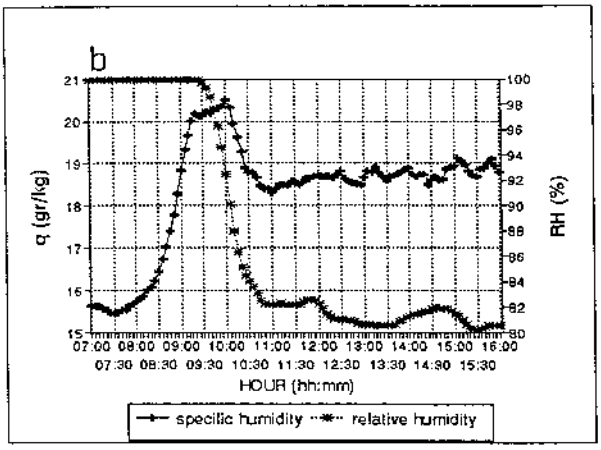

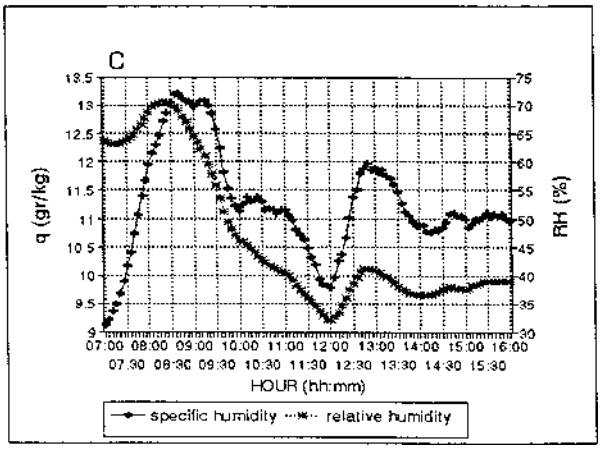

FIG. 6. Time series of specific humidity q (g kg^{-1}) and RH (%) at (a) ASD, (b) ASK, and (c) KG for 20 Jul 1993.

3) Temperature. Beginning of a decrease or a stabilization (stops increasing) for at least 15 min.
4) Relative humidity. Beginning of an increase or a stabilization for at least 15 min (section 3c).
5) Turbulence intensity. Point of maximum turbulence intensity (section 3b).

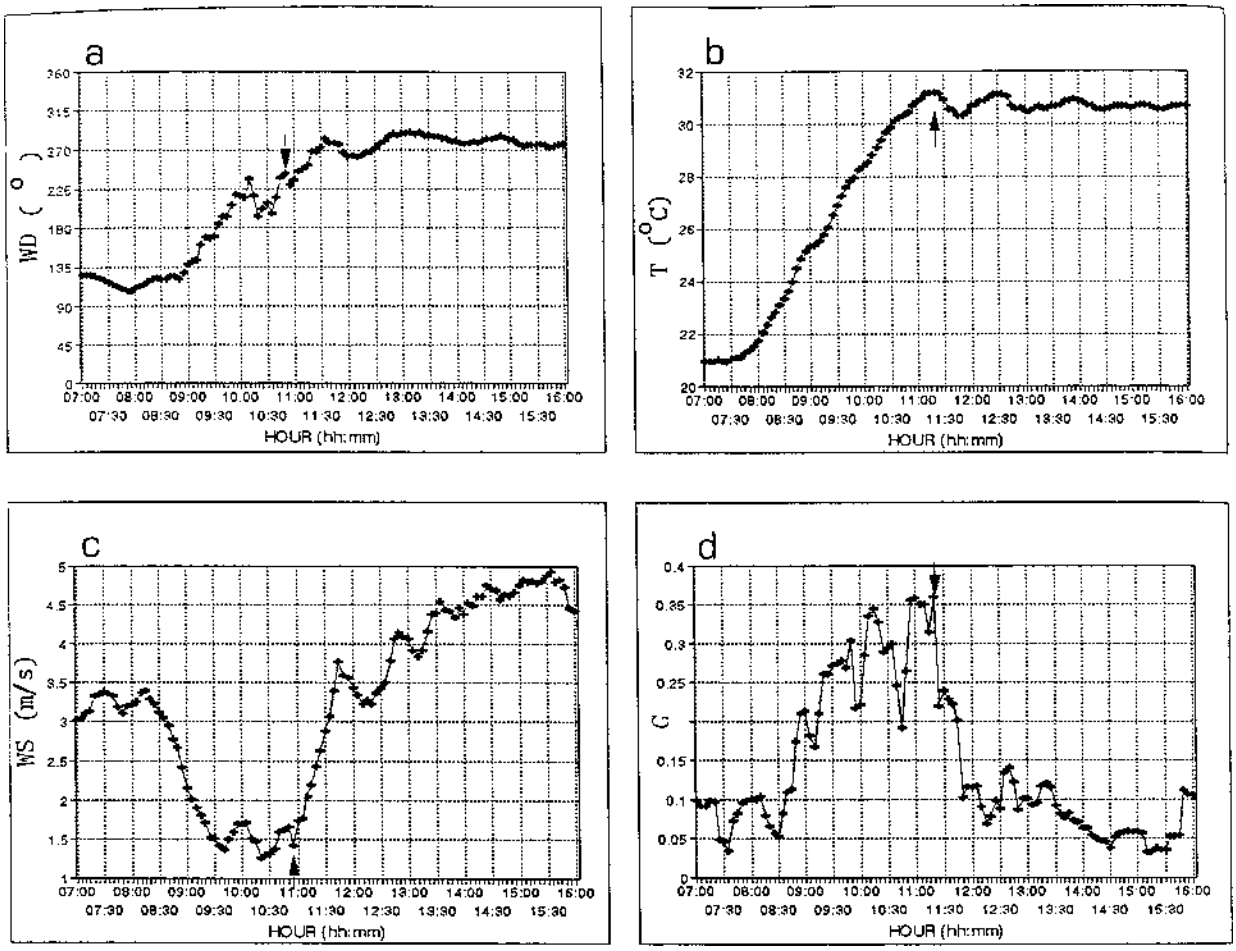

FIG. 7. Time series at GV for (a) wind direction (degrees), (b) temperature (°C), (c) wind speed (m s^{-1}), and (d) gustiness. All time series are on 20 Jul 1993.

For the aforementioned example of NI on 20 July 1993, criteria 1–3 yield SBF arrival times of 1045, 1045, and 1100 LST, respectively. Several problems related to the aforementioned criteria will be discussed later in section 3d.

b. Turbulence intensity as an additional criterion

Since most stations had only three regularly observed parameters, namely, wind direction, wind speed, and temperature, it was found useful to introduce an additional parameter: the turbulence intensity or gustiness (G).

Turbulence intensity may be defined as the ratio between the wind speed standard deviation, $\sigma = \sqrt{\overline{v'^2}}$, and the average wind speed $\overline{v}$, for example, Alpert and Eppel (1985),

$$G = \frac{\sqrt{\overline{v'^2}}}{\overline{v}} = \frac{\sigma}{\overline{v}}, \tag{1}$$

where v' is the instantaneous or turbulent wind taken as the 5-min basic measurement. It also is sometimes referred to gustiness, for example, Huschke (1959). It was calculated at each time based on the seven-point measurements (equivalent to 30-min time period) around the pertinent time. The 20-min gustiness values were too noisy. It should be noted that this is an approximate measure of turbulent intensity, since 5-min averages were adopted instead of instantaneous values. This can be a useful measure as illustrated by Alpert and Eppel (1985).

Figure 5 illustrates the G time series for the station NI as in Figs. 2–4. It shows a steady increase of G from about 0930 LST and the absolute maximum is reached at exactly 1100 LST, which fits well with the change in wind direction (Fig. 2b; 1045 LST), the change in wind speed (Fig. 3b; 1045 LST), and the decrease in temperature (Fig. 4b; 1100 LST).

Hence, a fifth criterion for the SBF is an absolute maximum in gustiness. This additional criterion has been inspected for all stations, and was found very useful in the objectively calculated decision-making in some problematic situations (section 3d). The theoretical basis for the increase of the wind turbulence at the SBF is beyond the scope of this paper. It is related to various instabilities

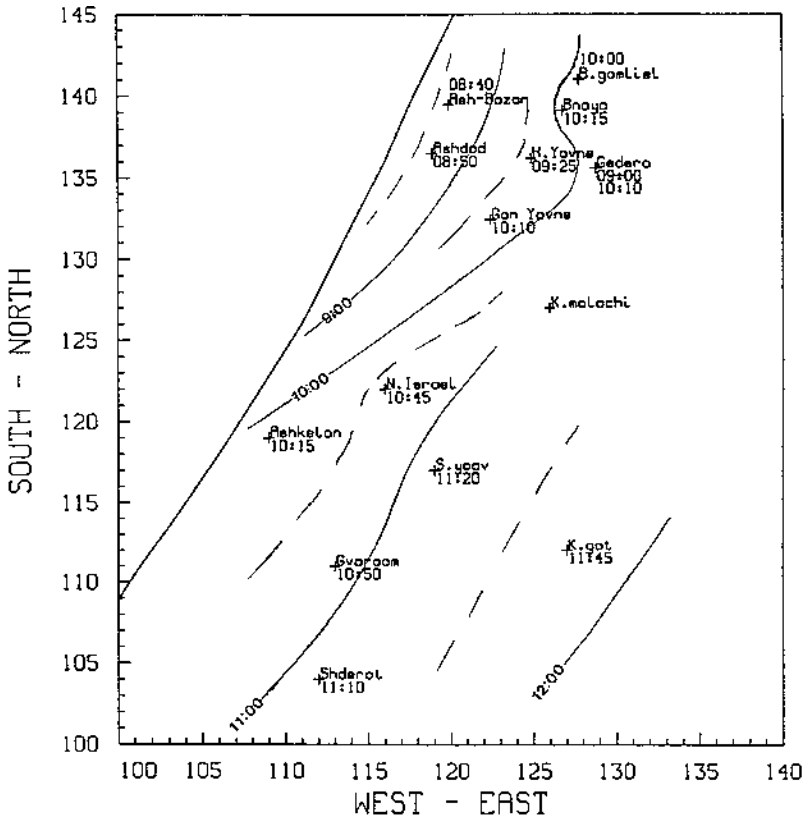

FIG. 8. The SBF arrival time isochrones for the 20 Jul 1993. Full (dashed) lines for full (half) hour isochrones. Times below each station indicate SBF passage time(s) according to the criteria derived.

associated with the steep SBF gradients such as Kelvin–Helmholz (KH) instability (section 5b).

c. Examination of the humidity criterion 4

Obviously, the relative humidity (RH) is closely associated with the temperature, as for instance, the RH may increase due to a temperature drop without any humidity increase. Consequently, the specific humidity q was calculated based on the following formula, for example Rogers and Yau (1989):

$$q = \frac{\mathrm{RH}}{100}\frac{R}{R_V}\frac{1}{p}Ae^{-B/T}, \qquad (2)$$

where $A = 2.53 \times 10^7$ hPa, $B = 5420$ K, T = temperature (K), $R = 287$ J kg^{-1} K^{-1} (gas constant), $R_V = 461$ J kg^{-1} K^{-1} (gas constant for water vapor), and p = pressure (hPa).

SBF arrival times with specific humidities (q) were found to be not much different from those defined with RH, but sometimes q serves as a better indicator for the SBF arrival. For instance, Figs. 6a–c show both q and RH at the ASD, ASK, and KG stations. In ASD (Fig. 6a) the tendencies are similar; both show small increases at 0730 LST (probably part of the break in the nocturnal surface inversion) with a more significant increase at 0855 LST associated with the SBF arrival. In ASK (Fig. 6b), however, the specific humidities increase sharply early in morning while RH stay at the maximum, of 100%. At 1000–1030 LST there is a sharp decrease in the specific humidity and the RH, which is probably related to break in the nocturnal inversion, for example, Segal et al. (1992). Only at 1050–1100 LST is there an increase in both the RH and q, which fits the other SBF criteria for the ASK station (not shown). Similar patterns are found in KG (Fig. 6c). Here, however, the SBF arrival at 1200 LST is recognized by a much sharper increase in the specific humidities as well as the RH. In the following, the RH was used in spite of some advantage to the specific humidity, because the pressure required calculating q, Eq. (2), was measured only at three stations as outlined in section 2a.

d. Objective detection of the SBF-associated problems

At each station, four (or five, when humidity was available) SBF arrival times according to the aforementioned four (five) criteria, were defined. If all times were within 1 h, the earliest time was chosen. Figures

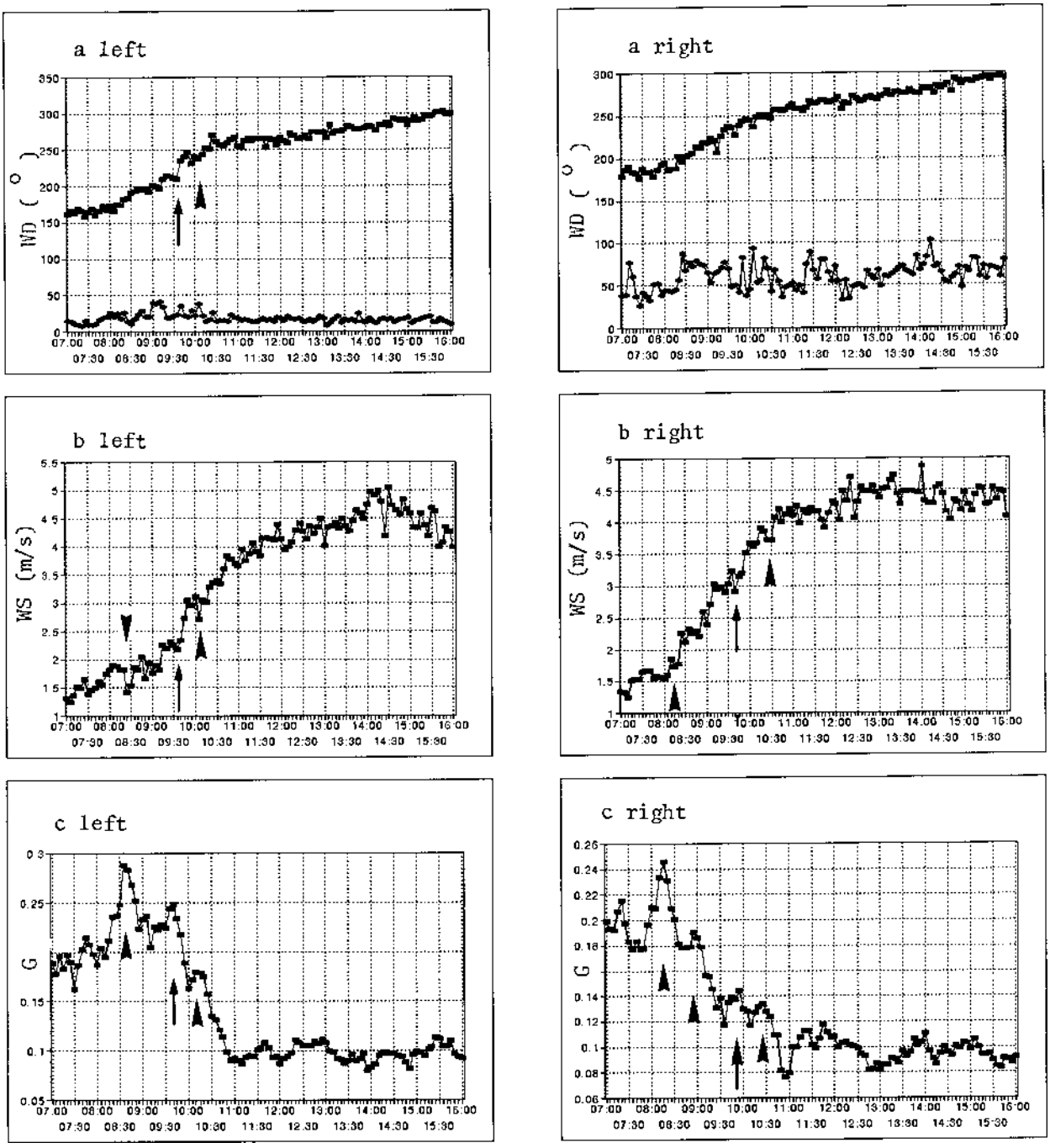

FIG. 9. Averaged time series for (left) 18–25 Jul 1993 and (right) for 20–28 Jul 1994 at ASK. The fields are based on 20-min averages for (a) WD, (b) WS, (c) *G*, (d) *T*, and (e) RH. In (a), the lower plots are the interdaily wind direction standard deviations. Arrows and arrowheads indicate SBF and pre- and post-SBF lines, respectively.

7a–7d, for instance, show the corresponding four figures for the station Gvaraam (GV); humidity was not available. According to the wind direction criterion, SBF arrival was at 1050 LST (Fig. 7a). Similarly, the temperature, wind speed and gustiness (Figs. 7b,c,d) yielded the times of 1120, 1105, and 1120 LST, respectively. Hence, the chosen SBF arrival time at GV was 1050 LST. Another example was given in section 2b for the NI station (Figs. 2–5).

In calculating all the criteria there are several problems besides those that are related to the quality of the data. First, the gustiness parameter may become large even without considerable fluctuations such as when the average wind is very weak [$\overline{v}$ close to 0 in Eq. (1)],

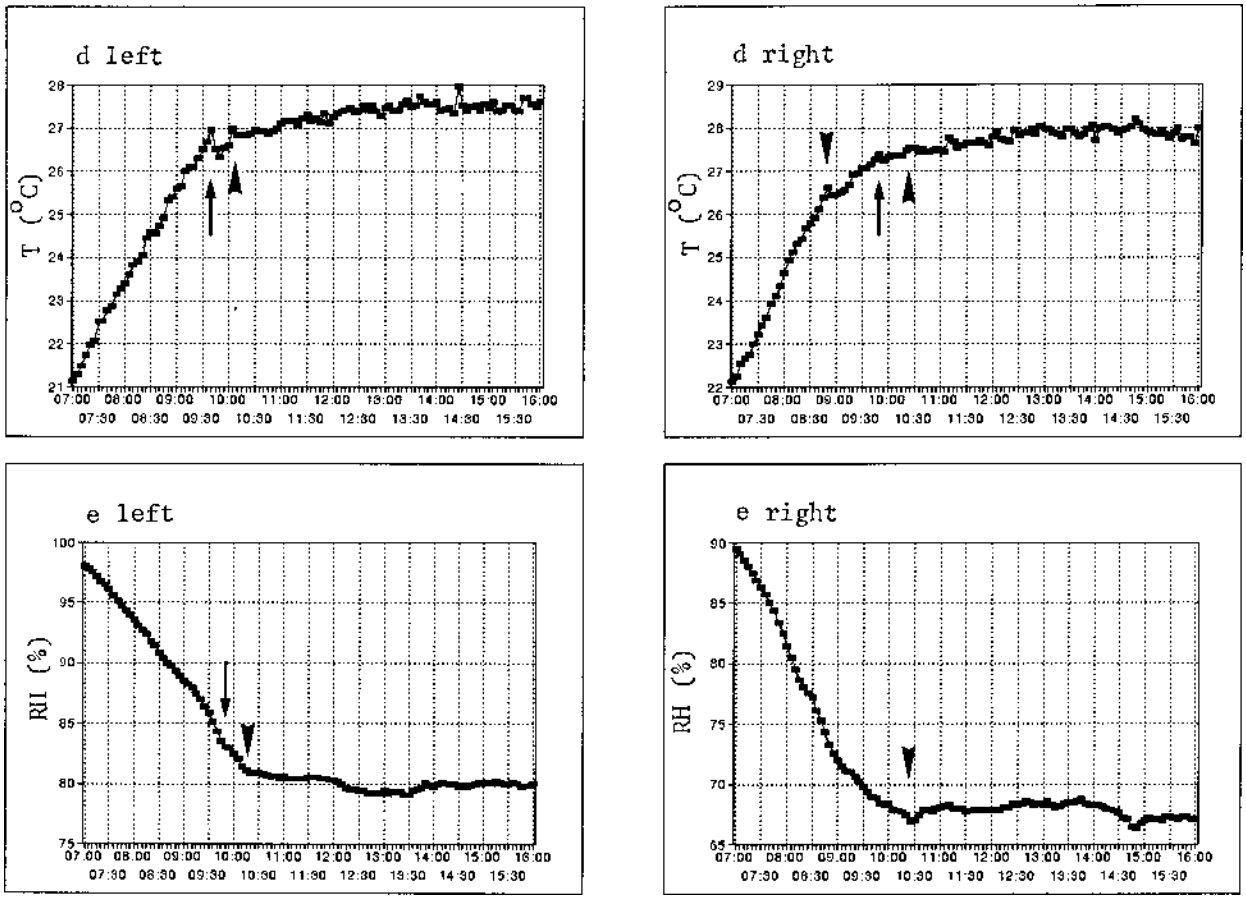

FIG. 9. (*Continued*)

along with even a weak change in a wind speed. Hence, there are *G* peaks that may not be related to the SBF.

Second, in some stations for some days the wind veering is too slow to obey criterion 1. This was the reason for modifying criterion 1 to the largest clockwise rotation that was found steady within 15 min. For very gradual turning, such a criterion may not be useful. In some cases the other criteria were also questionable but frequently when only this wind-veering difficulty occurred, it may have been related to an instrumental problem.

Third, in summer, wind turning was indeed always clockwise but in the transition seasons, when anticlockwise rotation may occur (due to a change in the synoptic forcing), the criterion was modified to the time when turning to the west or northwest sector arrived.

A fourth problem relates to effect of large cloud fraction, since even a small cloud fraction may significantly influence the screen temperature, for example, Segal and Feingold (1993). With larger cloud fraction, the other criteria may also be strongly affected. However, only four stations carry global radiation from which cloud fraction was inferred. Hence, the analysis on cloudy days became complicated and such days, which are rare over our study region of south Israel, were filtered out.

Sometimes, a retrograding sea breeze was observed. This may happen when the sea breeze opposes the synoptic gradients but is quiet rare during summer. Such a winter case, however, was simulated and discussed by Alpert et al. (1988, Fig. 2). Here, focus was given to summer cases where these situations are extremely rare.

In cases where two parameters supported one arrival time and the other two points another time, both arrival times were plotted. Finally, SBF arrival times for all stations were plotted on a geographic map, and isochrones for SBF arrival time were drawn. Figure 8, for instance, shows the SBF arrival time isochrones for the 20 July 1993. It shows that the SBF enters first over the northern section at about 0830 LST. The rate of SBF propagation inland increases as the SBF penetrates inland and will be discussed (Figs. 11, 12). Also, the potential reasons for the earlier arrival at the northern section will be discussed in section 4d.

4. Characteristics of the summer sea-breeze fronts and their pre and post lines

a. Observations for a specific day

In the daily examples shown so far, one may notice additional weaker lines ahead of and in the wake of the

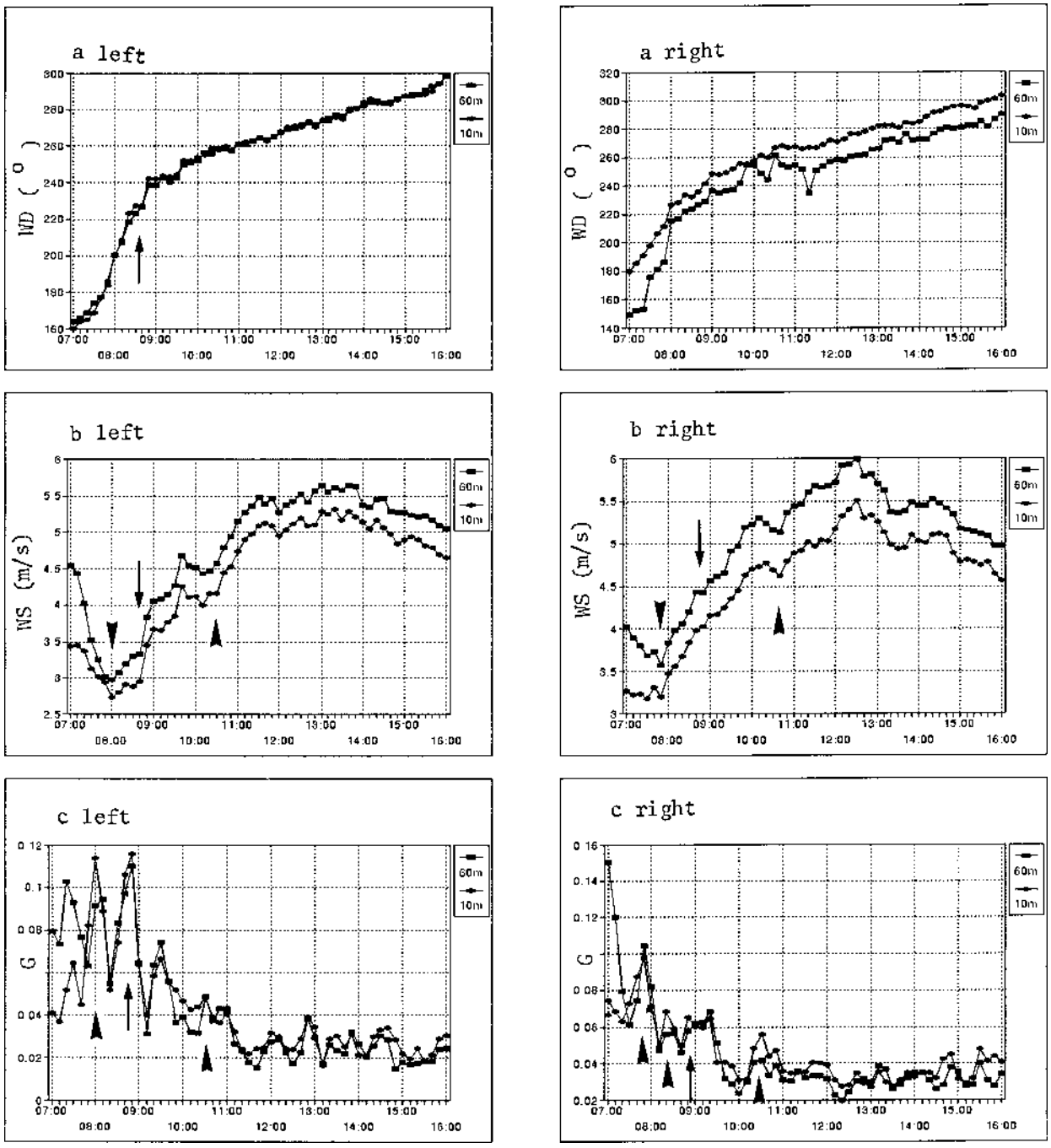

FIG. 10. As in Fig. 9, but for the tower station ASB at altitudes of 10 (dark filled plusses) and 60 m (dark rectangles) above ground. Arrows and arrowheads indicate the main SBF and pre- and post-SBF lines, respectively, that are described in the text.

SBF. For instance, at NI (Figs. 2–4, and Fig. 5) besides the identified dominant SBF at 1045–1100 LST, there exist two pre-SBF lines at about 0840 and 0940–0950 LST clearly noticed by the wind direction (Fig. 2b), the wind speed (Fig. 3b), and by the secondary maxima in the gustiness (Fig. 5). These are clearly noticed in the nonaveraged temperature (Fig. 4a), and also as breaks in the steep slope of the smoothed temperature increase at 0840 and 0950 LST (Fig. 4b).

A post-SBF can also be identified at about 1h after the passage of the primary SBF, that is, at about 1210 LST. In terms of the various parameters, the exact times are 1200 LST (WD), 1210 LST (WS), 1215 LST (T) and 1155 or 1215 LST (G). Similarly, at station GV

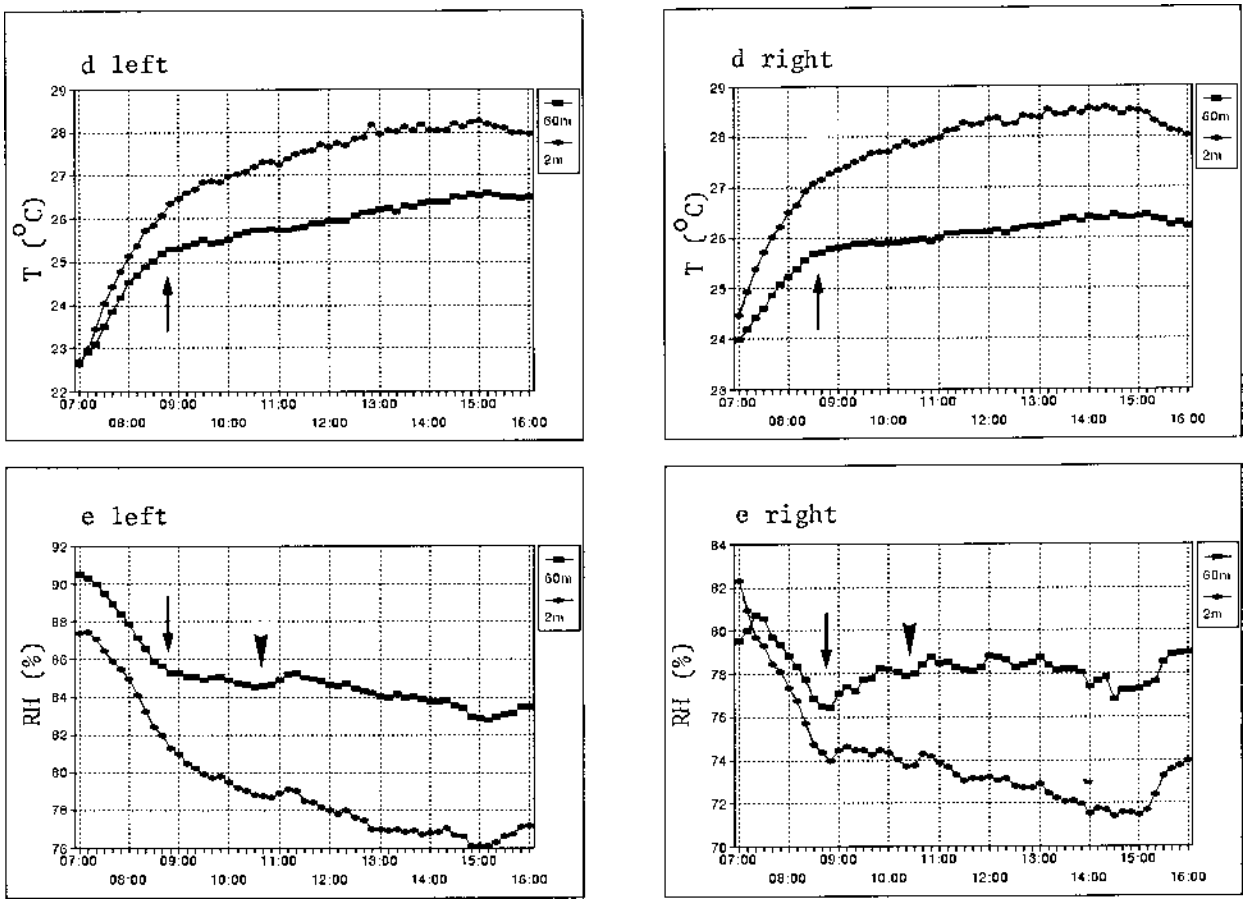

FIG. 10. (*Continued*)

one can clearly notice additional pre- and post-SBF lines. Since these lines are weaker than the dominant SBF, they may sometimes be more easily noticed in the nonaveraged fields, and the aforementioned criteria need to be less stringent. The pre- and post-SBF lines are indicated in Figs. 2–5 by arrowheads.

Are these lines due to turbulence of large eddies or are they consistent pre- and post-SBF lines dynamically associated with the SBF? Do they carry any consistent features?

b. Observations for periods of several days

This will be examined next by inspecting the SBF character over a period of 8 consecutive days in 1993 (18–25 July) and also for 9 days in 1994 (20–28 July). The averaging for the 8 or 9 days was performed every 5 min at each station and for all the parameters. We may consider this as a semiclimatological analysis of the July SBF. It is striking that besides the primary SBF, there are indeed pre- and post-SBF converging lines that are clearly noticed and are supported by either all the parameters or some of them. The pre-SBF lines found here may be related to the forerunners predicted in the theoretical study of Geisler and Bretherton (1969), and the post-SBF lines to the KH waves discussed by Sha et al. (1991; see section 5b). Before presenting the results, we note, first, that the convergence lines are well picked out by the gustiness *G*. Second, since this is a multiday average, the exact SBF criteria defined earlier for a single day cannot strictly apply but the search for the SBF features is performed similarly. Also, note that a small time correction of 5–7 min due to the progression of the sunrise time in late July through the 8 or 9 days was not applied.

In addition, we have calculated the interdaily standard deviation of the wind direction (SIGD) for each station. We expect to find a stronger SIGD at times, straddling around the expected SBF arrival, as is indeed observed, for example, Fig. 2a for NI. But, this time interval with maximum variability is also influenced by both the interdaily synoptic variations, though small, and the aforementioned gradual change in the solar angle. The interdaily variation (Fig. 9a) is strongly related to—but is clearly different from—the variation of the wind direction at a station around the SBF arrival time.

Figure 9 presents time series at ASK for July 1993 and 1994 for 8- and 9-day averages, respectively. The

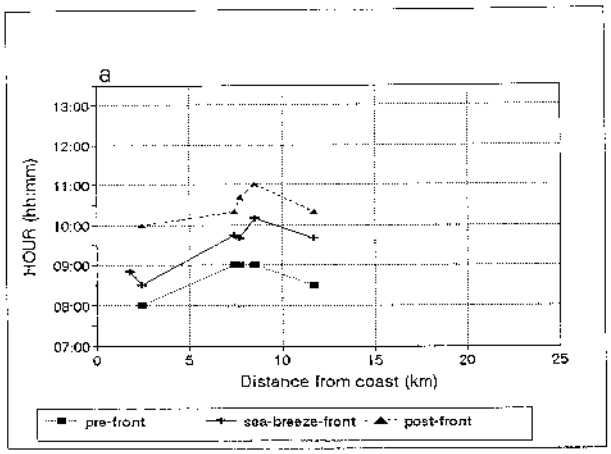

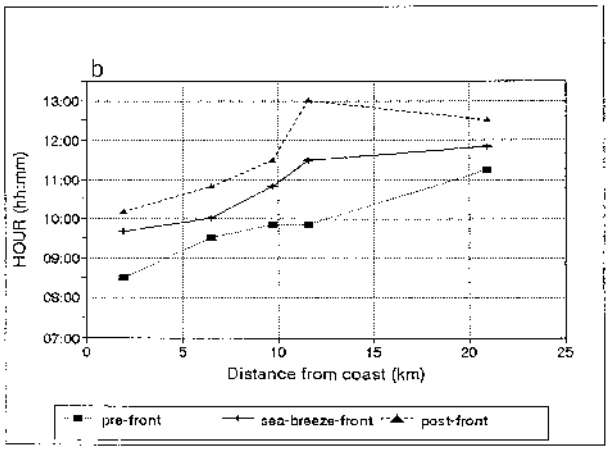

FIG. 11. Passage times for SBF, (plusses) and its pre- (rectangles) and post-SBF lines (triangles) as functions of distance from the coast (km): (a) for the northern cross section with stations ASD, GY, HY, BG, and GD; (b) for the southern cross section with stations ASB, ASK, NI, GV, SY, and KG; based on Jul 1993 averages.

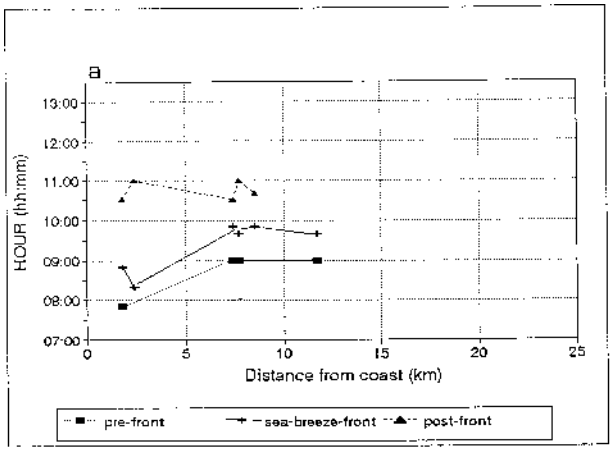

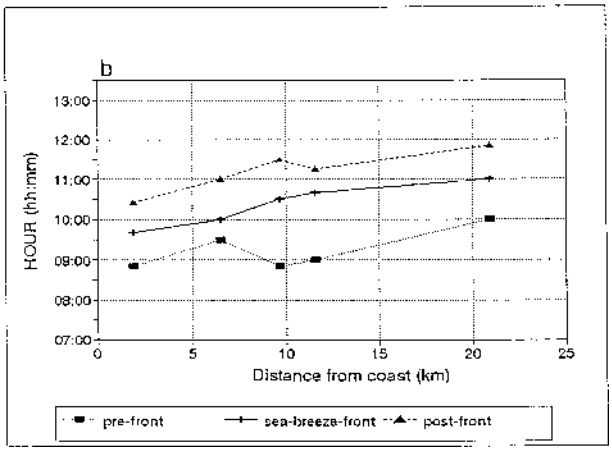

FIG. 12. As in Fig. 11, but for Jul 1994 averages.

interdaily wind direction standard deviation SIGD is plotted in the top panel for the WD series (the line at the bottom of Fig. 9a left and right). The two panels from top down are WD (and SIGD), WS, *G*, *T*, and RH; the left panels are for 1993, and the right for 1994. Following the detection criteria discussed in section 3, about four lines of convergence can be identified by some or all of these criteria. At around 0720 LST, about 1–2 h past sunrise, we can notice a small peak in the turbulence intensity *G*. Features are also found in SIGD and WS at this time and probably indicate the break of the aforementioned early-morning surface inversion. The more pronounced first convergence line, probably pre-SBF, is noticed at about 0815–0850 LST. In 1993 (left), it is detected by the significant maximum *G* at 0835 LST, and some strengthening of WS at 0825 LST. In 1994, *G* maxima are at 0815 and 0855 LST, strengthening of WS is at 0815 LST, and there is a light drop of *T* at 0850 LST. The main front passage is indicated by an arrow, while pre- and post-SBF lines are indicated by arrowheads.

The second most noticeable convergence line can be identified at 0940–0950 LST as the main SBF. It is clearly detected by *G*, WS, WD, *T*, and even by some weakening in the sharp decrease of the relative humidity.

The third converging line, post-SBF, is found at 1010–1025 LST in both 1993 and 1994 panels, and is strongly supported by the relative humidity and temperature (RH and *T*) but can also be noticed in *G* and WS.

The fact that the three converging lines including the pre- and post-SBF lines do appear even in averages of 8 or 9 summer days in 2 yr supports the significance of the pre- and post-SBF lines; lines that have so far received little attention in the extensive literature on sea breezes.

c. Tower observations

Further support for the existence of the pre- and post-SBF lines is provided by a similar analysis of the pa-

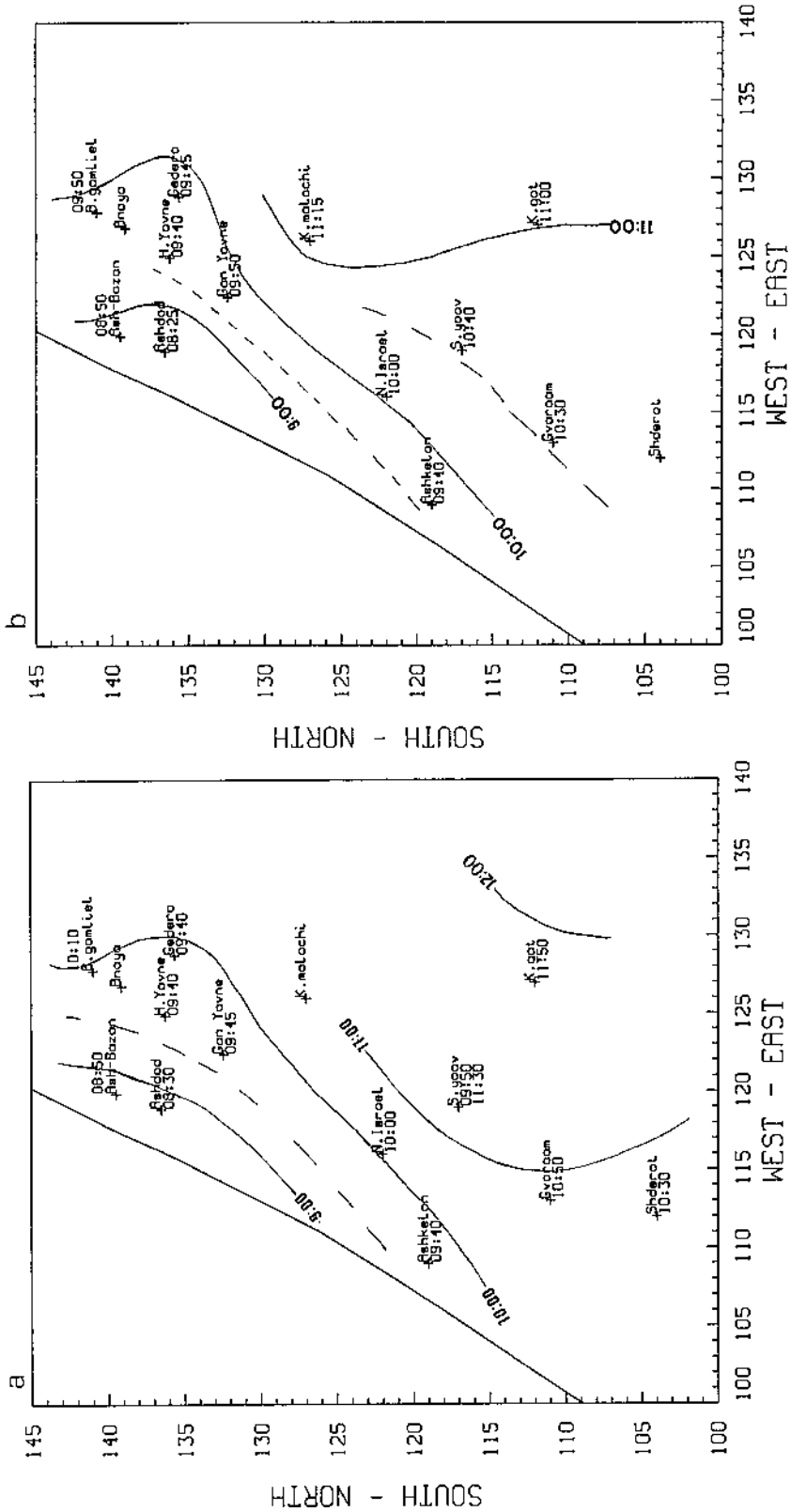

FIG. 13. As in Fig. 8, but for the average isochrones. Map is based on (a) Jul 1993 period and (b) Jul 1994 period.

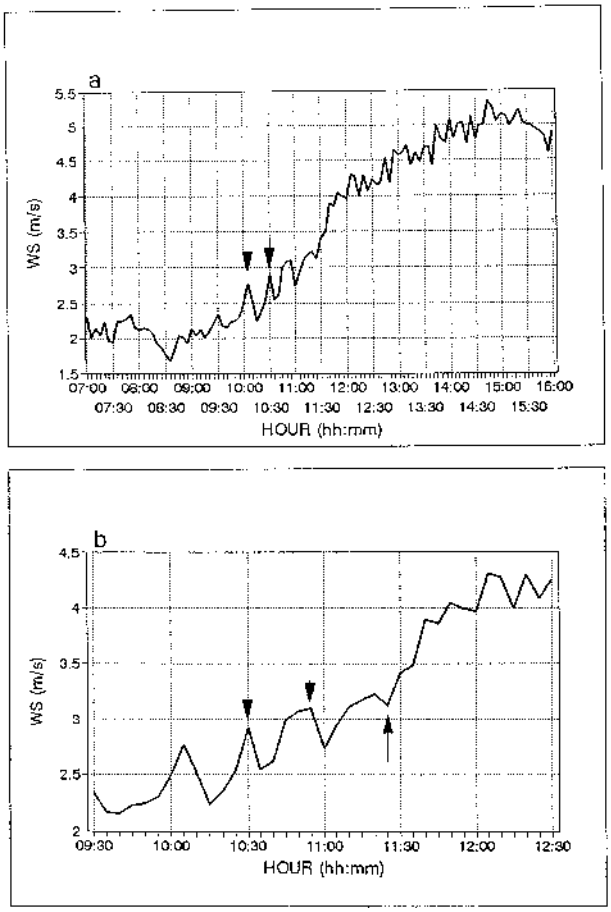

FIG. 14. (a) The wind speed at station SY, as a function of time, for the average period of Jul 1993. (b) A zoom over the relevant time period. The arrowheads show the pre-SBF lines, while the arrow indicates the SBF passage time.

rameters at the meteorological tower at ASB (for geographic location see Fig. 1) plotted in Fig. 10. Figures 10a–10c show the graphs at two altitudes of the tower, 10 and 60 m; Figs. 10d,e show graphs at 2 and 60 m for *T* and RH. The largest differences between the near surface and 60 m are for temperature and relative humidity. For instance, the surface temperature and RH react faster and stronger compared to their values at 60 m.

Here again, three convergence lines can be noticed. The first pre-SBF line appears at 0750–0810 LST. The winds veer quickly from south-southeast to southwest. The pre-SBF line is supported by WD, *G*, and also WS. The SBF can be identified by all the parameters at 0850 LST. The post-SBF line appears at 1030 LST and is supported by *G*, WS, RH, and *T*.

d. Inland propagation of the SBF and its associated frontal lines

Figures 11a,b and 12a,b show the inland propagation of the convergence lines as observed at the stations, plotted as the front passage time as a function of distance from the coast for the northern (top) and southern (bottom) sections of the study domain for 1993 and 1994, respectively. The slope of the line is the reciprocal of the propagation speed of the convergence lines. The propagation speed for all the frontal lines is of about 1.5–3 m s^{-1} near the coast, while further inland—at 10–20-km distance—speeds increase to about 3–10 m s^{-1}. This fits earlier reports in other regions, for example, Simpson (1977) and Fosberg and Schroeder (1966).

These SBF speed estimates are not accurate since the stations are not on a line exactly perpendicular to the coast and the SBF propagation inland is clearly not uniform along the coast. Also, there is some deflection inland due to Coriolis force as discussed earlier. This is illustrated in Figs. 13a,b, where the SBF average isochrones are plotted over the study region (the figure also explains the impossible negative slopes in some sections of Figs. 11a and 12a,b). It is interesting to see that the SBF passage times for 1993 and 1994 are nearly the same at most of the stations. This illustrates the overall dominance of the local sea-breeze forcing as compared to the synoptic forcing. The synoptic effects on the SBF seem to be responsible for the differences between the propagation of the (late July) average SBF. As may be expected, this synoptic difference is more pronounced inland. The maximum difference in the SBF passage is 50 min at the station KG (Fig. 1); that is, it is 1150 LST for July 1993 and 1100 LST for July 1994. The faster frontal lines in 1994, as compared to 1993, fits stronger large-scale westerlies and is consistent with theoretical expectations (e.g., Arritt 1993).

Another interesting feature is the 1-h earlier arrival of the SBF at the northern section—ASD and ASB (Fig. 1) area. This is true for both years and appears also in our mesoscale model simulations, for example, Alpert and Getenio (1988). The reason for this is not completely clear and it is perhaps due to the differences in the curvature in the coastline (Neumann 1951), topography, land cover, etc. This requires further study.

5. Further discussion on the pre- and post-SBF lines

a. The pre-SBF line

In the preceding section we have described pre- and post-SBF lines for specific summer days and also for field averages of 8 or 9 consecutive July days. Their signatures were most discernible in the turbulence and wind speed, less so in the wind veering, particularly for the post-SBF lines.

Geisler and Bretherton (1969, hereafter GB) analytically described the SBF. It was represented by the solution of the thermodynamic equation with a prescribed heating as an instantaneous spatial discontinuity in the temperature over a layer with uniform height *h* over land. The heat equation becomes

$$\frac{\partial \sigma'}{\partial t} + N^2 w = g\frac{\theta_0'}{\overline{\theta}_m}\delta(t)H(x)H(h - Z), \qquad (3)$$

where x is the direction perpendicular to the coast, $N^2 = (g/\overline{\theta}_m)(\partial\overline{\theta}/\partial z)$ is the Brunt–Väisälä frequency, and $\sigma' = -g\rho'/\rho_m = g\theta'/\overline{\theta}_m$ is the buoyant force. The right-hand side of Eq. (3) represents the thermal forcing of the initial perturbation $\delta(t)$, where θ_0' is the potential temperature perturbation at time $t = 0$; $\overline{\theta}_m$ is the average potential temperature; and $H(X)$, $H(h - Z)$ are step functions that define the atmospheric layer over land where the heating is imposed. Subscript m denotes the mean value and w is the vertical velocity. The perturbed solution was found to propagate as gravity waves ahead of the front that were entitled by GB as forerunners. Geisler and Bretherton (1969) plotted the wind speed in the forerunners as function of their distance from the SBF (GB, Fig. 5). For an imposed heating function depth h of 1 km, this speed was about 1 m s^{-1}. Next, we will try to correlate GB predictions to our results for the pre-SBF lines. According to GB, the forerunner is roughly estimated to reach a point 10 km inland in about 30–50 min after the SBF crossed the coastline.

Comparing the SBF timing in ASK, near the coast and the wind speed in Sde-Yoav (SY), about 10 km east of ASK for the July 1993 average, we find that the pre-SBF line at SY occurs about 30 min after the SBF at ASK. The SBF passed ASK at 0940 LST (Fig. 9, WS) while the pre-SBF line in SY (based on wind maximum, following GB) was at 1005 or 1030 LST. Figure 14 shows the wind speed in SY for average July 1993. The lower panel is a zoom on the relevant time window. The arrowheads show the pre-SBF line while the arrow shows the SBF passage in SY. Notice that, in Fig. 11b, the location of the pre-SBF line in SY is earlier—at about 0955 LST—because it is based on our WS criterion not the maximum WS, as in GB. On specific days the identification of the frontal lines is easier.

It should be noted that in aircraft observations of the sea-breeze (SB) circulation, one can notice pre-SBF lines to the main SBF (Finkele et al. 1995, Fig. 4). The typical wind intensification across these lines is about 1 m s^{-1} corresponding to both GB predictions and our observations (Fig. 14).

b. The post-SBF line

Sha et al. (1991, Fig. 4) have shown in a numerical simulation that the KH instability is responsible for KH secondary waves following the SBF. Although the KH waves are most prominent at an altitude of several hundred meters where the horizontal sea-breeze wind vanishes, the signature of the waves can be noticed also at the surface in the temperature, wind, and pressure.

Such a wavy character is also found in our results, primarily in the temperature field and sometimes in the wind speed. For example, Figs. 3 and 4 show the temperature and wind speed in NI on the 20 July 1993. The SBF is indicated by the arrow at 1040 and it is followed by strong waves. Another example for the same day is from GV station, Fig. 7, in both temperature and wind speed. This seems in some contrast to Sha et al.'s simulation in which the wavelike variation is in velocity and pressure but not in the potential temperature.

In the summer averages, these waves tend to partly cancel out and it is therefore more difficult to identify the post-SBF lines. The post-SBF lines are frequently noticed in the humidity and turbulence fields, much less with the wind direction.

6. Summary

This work presents a meso-γ-scale station analysis of the summertime sea breezes over the south coastal plane of Israel employing high spatial and temporal near-surface resolutions.

We have formulated objective criteria for the SBF passage based on wind speed/direction, temperature and relative humidity. This suggests the possibility of producing a computer operational warning system as, for instance, in relation to pollutant dispersion. The relationship between the pre- and post-SBF lines and pollutant transport was explored by Rabinovich-Hadar (1995). The paper focuses on summer cases where the synoptic forcing is quite steady (Alpert et al. 1992), therefore allowing a very detailed inspection of the SBF characteristics.

The criteria included fast veering of the wind, significant increase of wind speed, temperature decrease, humidity increase and maxima in the turbulence intensity. The criteria were found to be reliable on clear days. The most convenient criteria for the SBF were found to be the specific humidity, temperature and turbulence intensity.

As well as the primary SBF, we have found pre- and post-SBF lines. This finding was not reported earlier as steady phenomena for many summer days. It is important for pollutant transport, human comfort, and, in general, for a more fundamental understanding of the SB phenomenon. There are some theories suggesting possible mechanisms to explain secondary frontal lines like the GB forerunners or the Sha et al. (1991) Kelvin–Helmholz waves. In presenting our pre- and post-SBF lines analysis to C. Ramis, it was pointed out that a trace of post-SBF line can also be noticed in Mallorca observations in Spain (Ramis et al. 1990). These frontal lines can be also noticed in Finkele et al. (1995) aircraft observations.

Our study suggests that the most convenient field to identify the secondary SBF lines is the turbulence intensity followed by wind speed. Temperature is also useful for detecting the post-SBF lines. It is difficult to notice any significant wind veering associated with the secondary lines.

Acknowledgments. Thanks to the Town Municipalities for the Environmental Monitoring in Ashdod and Ashkelon, and especially to D. Lahav, Yuval, and Uri for help with the data. Thanks to the Israel Meteorological Service for the meteorological data. Support to this research was given by Ministry of Environment through the Israel Electric Company, and partly by GLOWA-JR, MOS-BMBF, and the EC DETECT projects. Thanks to H. Shafir for final editing of the article, and to E. Heifetz, I. Machat and S. Tetro for assisting in the study. Thanks to the reviewers for their constructive suggestions.

REFERENCES

Alpert, P., 1988: The combined use of three different approaches to obtain the best estimate of meso-beta surface winds over complex terrain. *Bound.-Layer Meteor.,* **45,** 291–305.

——, and E. Eppel, 1985: A proposed index for mesoscale activity. *J. Climate Appl. Meteor.,* **24,** 472–480.

——, and B. Getenio, 1988: One-level diagnostic modeling of mesoscale surface winds in complex terrain. Part I: Comparison with three-dimensional modeling in Israel. *Mon. Wea. Rev.,* **116,** 2025–2046.

——, A. Cohen, J. Neumann, and E. Doron, 1982: A model simulation of the summer circulation from the eastern Mediterranean past Lake Kinneret in the Jordan valley. *Mon. Wea. Rev.,* **110,** 994–1005.

——, M. Kusuda, and N. Abe, 1984: Anticlockwise rotation, eccentricity, and tilt angle of the wind hodograph. Part 2: Observational study. *J. Atmos. Sci.,* **41,** 3558–3573.

——, B. Getenio, and R. Zak-Rosentahl, 1988: One-level modeling for diagnosing surface winds over complex terrain. Part II: Applicability to short-range forecasting. *Mon. Wea. Rev.,* **116,** 2047–2061.

——, R. Abramsky, and B. U. Neeman, 1992: The prevailing summer synoptic system in Israel—Subtropical high, not Persian trough. *Isr. J. Earth Sci.,* **39,** 93–102.

Arritt, R. W., 1993: Effects of the large-scale flow on characteristic features of the sea breeze. *J. Appl. Meteor.,* **32,** 116–125.

Atkinson, B. W., 1981: *Mesoscale Atmospheric Circulation.* Academic Press, 495 pp.

Chiba, O., 1993: The turbulent characteristics in the lowest part of the sea breeze front in the atmospheric surface layer. *Bound.-Layer Meteor.,* **65,** 181–195.

Clarke, R. H., 1955: Some observations and comments on the sea breeze. *Aust. Meteor. Mag.,* **11,** 47–52.

Estoque, M. A., 1962: The sea breeze as a function of the prevailing situation. *J. Atmos. Sci.,* **19,** 244–250.

Finkele, K., J. M. Hacker, H. Kraus, and R. A. D. Byron-Scott, 1995: A complete sea-breeze circulation cell derived from aircraft observations. *Bound.-Layer Meteor.,* **73,** 299–317.

Fosberg, M. A., and M. J. Schroeder, 1966: Marine air penetration in central California. *J. Appl. Meteor.,* **5,** 573–589.

Geisler, J. E., and F. P. Bretherton, 1969: The sea-breeze forerunner. *J. Atmos. Sci.,* **26,** 82–95.

Haurwitz, B., 1947: Comments on the sea-breeze circulation. *J. Meteor.,* **4,** 3–8.

Helmis, C. G., D. N. Asimakopoulos, D. G. Deligiorgi, and D. P. Lalas, 1987: Observations of sea breeze fronts near the shoreline. *Bound.-Layer Meteor.,* **38,** 395–410.

Huschke, R. H., Ed., 1959: *Glossary of Meteorology.* American Meteorological Society, 638 pp.

Kimble, G. H. T., 1946: Tropical land and sea breezes. *Bull. Amer. Meteor. Soc.,* **27,** 99–113.

Kusuda, M., and P. Alpert, 1983: Anticlockwise rotation of the wind hodograph. Part I: Theoretical study. *J. Atmos. Sci.,* **40,** 487–499.

Neumann, J., 1951: Land breezes and nocturnal thunderstorms. *J. Meteor.,* **8,** 60–67.

——, 1977: On the rotation rate of the direction of sea and land breezes. *J. Atmos. Sci.,* **34,** 1913–1917.

——, and Y. Mahrer, 1971: A theoretical study of the land and sea breeze circulation. *J. Atmos. Sci.,* **28,** 532–542.

——, and ——, 1974: A theoretical study of the sea and land breezes of circular islands. *J. Atmos. Sci.,* **31,** 2027–2039.

Pearce, R. P., 1955: The calculation of a sea breeze circulation in terms of the differential heating across the coast line. *Quart. J. Roy. Meteor. Soc.,* **81,** 351–381.

Rabinovich-Hadar, M., 1995: Sea breeze front structure and characteristics at the southern coast of Israel (in Hebrew). M.Sc. thesis, Dept. of Geophysics and Planetary Science, Tel-Aviv University, 102 pp.

Ramis, C., A. Jansa, and S. Alonso, 1990: Sea breeze in Mallorca. A numerical study. *Meteor. Atmos. Phys.,* **42,** 249–258.

Rogers, R. R., and M. K. Yau, 1989: *A Short Course in Cloud Physics.* Pergamon Press, 293 pp.

Schroeder, M. J., M. A. Fosberg, O. P. Cramer, and C. A. O'Dell, 1967: Marine air invasion of the Pacific coast: A problem analysis. *Bull. Amer. Meteor. Soc.,* **48,** 802–807.

Segal, M., and G. Feingold, 1993: Impact of local convective cloud systems on summer daytime shelter temperature. *J. Appl. Meteor.,* **32,** 1569–1578.

——, Y. Mahrer, R. A. Pielke, and R. C. Kessler, 1985: Model evaluation of the summer daytime induced flows over southern Israel. *Isr. J. Earth Sci.,* **34,** 39–46.

——, G. Kallos, J. Brown, and M. Mandel, 1992: Morning temporal variations of shelter-level specific humidity. *J. Appl. Meteor.,* **31,** 74–85.

Sha, W., T. Kawamura, and H. Ueda, 1991: A numerical study on sea/land breeze as a gravity current: Kelvin–Holmholtz billows and inland penetration of the sea-breeze front. *J. Atmos. Sci.,* **48,** 1649–1665.

Simpson, J. E., 1994: *Sea-Breeze and Local Winds.* Cambridge University Press, 228 pp.

——, D. A. Mansfield, and J. R. Milford, 1977: Inland penetration of sea breeze fronts. *Quart. J. Roy. Meteor. Soc.,* **103,** 47–76.

Skibin, D., and A. Hod, 1979: Subjective analysis of mesoscale flow patterns in northern Israel. *J. Appl. Meteor.,* **18,** 329–338.

Staley, D. O., 1957: The low-level sea breeze of northwest Washington. *J. Meteor.,* **14,** 458–470.

Wakimoto, R. M., and N. T. Atkins, 1994: Observations of the sea-breeze front during CaPE. Part I: Single-Doppler, satellite, and cloud photogrammetry analysis. *Mon. Wea. Rev.,* **122,** 1092–1113.